

The properties of the absorbing and line emitting material in IGR J16318-4848

Giorgio Matt¹ and Matteo Guainazzi²

¹*Dipartimento di Fisica, Università degli Studi “Roma Tre”, Via della Vasca Navale 84, I-00146 Roma, Italy*

²*XMM-Newton Science Operation Center, RSSD of ESA, VILSPA, Apartado 50727, E-28080 Madrid, Spain*

2 November 2018

ABSTRACT

We have performed a detailed analysis of the XMM–Newton observation of IGR J16318-4848, to study the properties of the matter responsible for the obscuration and for the emission of Fe and Ni lines. Even if the line of sight material has a column density of about $2 \times 10^{24} \text{ cm}^{-2}$, from the Fe $K\alpha$ line EW and Compton Shoulder we argue that the matter should have an average column density of a few $\times 10^{23} \text{ cm}^{-2}$, along with a covering factor of about 0.1–0.2. The iron $K\alpha$ line varies on time scales as short as 1000 s, implying a size of the emitting region smaller than about $3 \times 10^{13} \text{ cm}$. The flux of the line roughly follows the variations of the continuum, but not exactly, suggesting a variation of the geometrical properties of the emitting region on similar time scales.

Key words: line: formation; X–rays: binaries; X–rays: individual: IGR J16318-4818

1 INTRODUCTION

IGR J16318-4818 was discovered by the ISGRI detector of the IBIS instrument onboard the INTEGRAL satellite (Corvoisier et al. 2003) on January 29, 2003, with a 15–40 keV flux of 50–100 mCrab. It was initially interpreted as a new “transient” X-ray source. However, a reanalysis of archival ASCA data revealed the presence of a source whose position was coincident with that of IGR J16318-4818 (Murakami et al. 2003), and with a 2–10 keV observed flux of about $4 \times 10^{-11} \text{ erg cm}^{-2} \text{ s}^{-1}$.

The INTEGRAL discovery prompted a Target of Opportunity observation with XMM–Newton (Jansen et al. 2001) on February 10, 2003. The EPIC spectra unveiled a variable and strongly absorbed source, with evidence for strong emission lines (Schartel et al. 2003). This is in agreement with the ASCA source, in which Revnivtsev et al. (2003) suggested a column density $> 4 \times 10^{23} \text{ cm}^{-2}$. Preliminary spectral fits (de Plaa et al. 2003) indeed suggested that during the XMM–Newton observation IGR J16318-4818 was obscured by a Compton-thick absorber [$N_H = (1.66 \pm 0.16) \times 10^{24} \text{ cm}^{-2}$; all errors quoted hereinafter are at the 90% confidence level for one interesting parameter]. The emission complex could be resolved in three lines, with centroid energy of $6.410 \pm 0.003 \text{ keV}$, $7.09 \pm 0.02 \text{ keV}$ and $7.47 \pm 0.02 \text{ keV}$.

In this paper we exploit the unprecedented sensitivity of the EPIC detectors above 5 keV (where fluorescent transition of Fe and Ni are concentrated) to characterize the

physical properties of the matter responsible for the obscuration of the X-ray source and the associated reprocessing features. To achieve this goal, we compare the spectral fit results (presented and discussed in Sect. 3.1 of this Letter) with Monte-Carlo simulations of the X-ray transmission by neutral matter (Matt et al. 1999; Matt 2002; see Sect. 3.2), originally developed in the context of obscured AGN. We demonstrate in this paper that a proper modeling of the scattering effect is crucial to correctly identify the properties of the absorber, as standard fits with approximate model can grossly overestimate the actual absorbing column density and covering factor of the obscuring matter. Study of the spectral variability during the XMM–Newton observation allowed us to set stringent constraints on the geometry of the absorbing matter (see Sect. 3.3). Our findings and conclusions are summarized in Sect. 4.

2 DATA REDUCTION

In this paper, we discuss the pn data only (Strüder et al. 2001), as this instrument seems to be the best calibrated among the EPIC cameras (see, for instance, the discussion in Molendi et al. 2003), at least in their highest energy band.

Data were retrieved from the XMM–Newton Target of Opportunity public WEB page as Observation Data Files (ODF), and reprocessed with SAS v.5.4.1, using a calibration index file corresponding to the most updated calibration files available at February 21, 2003. Spectra were ex-

arXiv:astro-ph/0303626v1 28 Mar 2003

tracted from a circular region around the source centroid ($\alpha_{2000} = 16^h 31^m 48^s.6$, $\delta_{2000} = -48^\circ 49' 00''$; Schartel et al. 2003) with a $52''$ radius. As the extraction region encompassed two CCDs, background spectra were extracted from a nearby source-free region, having the same area ratio between the two chips as the source extraction region. We verified that the results are not substantially different, if the source and background pn spectra are extracted from a smaller region ($11''$ radius), fully comprised in the same CCD. The spectra were accumulated using single- and double-events. Pile-up is negligible, as well as the contribution of the background, lower than 0.1% in the 5–15 keV energy band. Nevertheless, a short interval of about 1.25 ks duration, where the background count rate (calculated on the single-event light curve extracted above 10 keV) exceeded 1 s^{-1} , was removed from the scientific product accumulation. The background is otherwise quite stable. The fits described in this Letter were performed with XSPEC v.11.1.

3 DATA ANALYSIS AND RESULTS

3.1 Time integrated spectrum: summary of spectral results

As already noted by de Plaa et al. (2003), the XMM-Newton spectra are characterized by a heavily absorbed continuum and 3 emission lines. The lines are most naturally interpreted as the Fe $K\alpha$ and $K\beta$ and the Ni $K\alpha$. We therefore fitted the spectrum (in the 5–13 keV energy band, as below 5 keV a small excess emission is present, see below) with the simplest possible model: an absorbed power law plus three (unabsorbed) narrow (*i.e.* intrinsic width, σ , fixed to 1 eV) Gaussian lines. The photoelectric absorption model VARABS has been used with element abundances from Anders & Grevesse (1989) and photoelectric cross sections from Balucinska-Church & McCammon (1992). We left the iron abundance free to vary independently of the other elements. As the absorbing matter results to be Compton-thick (see below), we included also Thompson absorption (model CABS). It is worth noting that this model, ignoring the scattering of photons, is, strictly speaking, valid only for absorbing matter along the line of sight with a negligible covering factor (see below for a discussion),

The fit is reasonably good ($\chi^2=99.1/64$ d.o.f.), but residuals around the iron $K\alpha$ line are visible, most likely due to the Compton Shoulder (CS), as already observed in the reflection spectrum of the Circinus Galaxy (Bianchi et al. 2002; Molendi et al. 2003), and expected on theoretical ground (see Matt 2002 and references therein). Modeling for simplicity the Compton Shoulder with a Gaussian with centroid energy fixed to 6.3 keV, and σ fixed to 50 eV, a significant improvement is found ($\chi^2=80.9/63$ d.o.f., corresponding to 99.96% confidence level). In the following we will refer to the complete model (absorbed power-law plus 4 Gaussian emission lines) as the *baseline model*. The best fit results are summarized in Table 1. The observed 2–10 keV flux is $6.7 \times 10^{-12} \text{ erg cm}^{-1} \text{ s}^{-1}$. The flux corrected for absorption is instead $1.1 \times 10^{-9} \text{ erg cm}^{-1} \text{ s}^{-1}$, corresponding to a luminosity of $1.3 \times 10^{37} d_{10}^2 \text{ erg s}^{-1}$, where d_{10} is the distance to the source in units of 10 kpc.

Given the large column density of the line-of-sight absorber, if the covering factor of the absorbing matter is large,

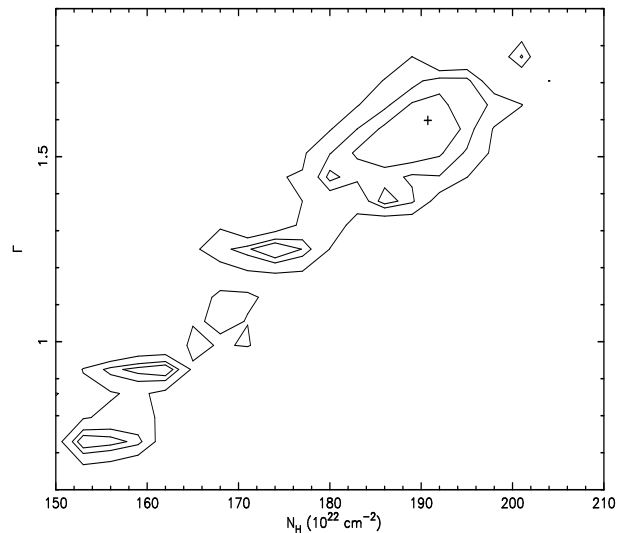


Figure 1. The Γ - N_{H} contour plot. The contours correspond to $\Delta\chi^2=2.3, 4.61$ and 9.21 .

a significant contribution from photons scattered towards the line of sight is expected, as discussed in Matt et al. (1999). We therefore fitted the spectrum with the Monte-Carlo model described in that paper. The fit is completely unacceptable. This may be due to the fact that the model has been calculated adopting the Morrison & McCammon (1983) cross sections, which made use of the Anders & Ebihara (1982) element abundances. In this set the iron abundance is about 0.7 times that given by Anders & Grevesse (1983), while from Table 1 it seems that the actual iron abundance (mainly derived in the fit from the depth of the iron edge) in the absorbing material is closer to the one given by the latter authors. Moreover, the Matt et al. (1999) model assumed spherical geometry and homogeneous matter, while the covering factor may be significantly smaller than one and the average column density smaller than that on the line-of-sight (see below).

Coming back to the results summarized in Table 1, we must first of all remark that the rather small errors on Γ and N_{H} are somewhat misleading. In fact, as it is clear from the contour plot (Fig. 1), the χ^2 distribution is shallow and not very smooth. The calculated errors correspond to the $\Delta\chi^2$ in the vicinity of the best fit, but other regions with $\Delta\chi^2$ less than 2.71 do exist. We have verified that N_{H} and A_{Fe} are only slightly correlated each other. To avoid problems in the estimate of the errors for the line parameters, we fixed Γ and N_{H} to their best fit values. This does not affect very much the errors on the Fe and Ni $K\alpha$ lines, but stabilizes the values for the Fe $K\beta$, which otherwise would be very difficult to find, due to its proximity to the iron edge.

3.2 The physical properties of the absorber

The energies of the Fe and Ni $K\alpha$ lines correspond to neutral or low ionized atoms (House 1969). On the contrary, the Fe $K\beta$ centroid energy is significantly larger than expected. This cannot be due to high ionization, not only because it does not agree with the $K\alpha$ energy, but also because for significantly ionized matter the $K\beta$ line becomes much fainter, to disappear completely for Fe XVII or more, when

no M electrons remain. Instead the observed $K\beta/K\alpha$ ratio ($0.20 \pm_{0.03}^{0.02}$) is slightly larger than expected for neutral iron (see the discussion in Molendi et al. 2003, where however the matter was seen in reflection, not transmission; the arguments given there must therefore be taken with caution, until proper calculations will be available). It should however be noted that, given the proximity to the iron edge, the parameters of the $K\beta$ line are necessarily difficult to estimate, and may suffer from a too simple modeling of the edge (Palmeri et al. 2002).

The Ni to Fe $K\alpha$ line ratio is about 6%, suggesting a possible Ni overabundance (see again the discussion in Molendi et al. 2003, with the same caution given above). In Table 1, the EW of the lines with respect to the unabsorbed continuum (to make easier the comparison with the expected value for the iron $K\alpha$ presented in Matt 2002), are also given. The value reported in Fig. 1 of Matt (2002) are for Morrison & McCammon (1983) abundances, and a power law index of 2. We therefore calculated the expected Fe $K\alpha$ properties using the code described in Matt (2002), adopting the Anders & Grevesse abundances and the best fit value for Γ , N_{H} , and A_{Fe} . The expected value of the ratio, f , between the Compton Shoulder and the line core is 0.44, to be compared with a measured value of $0.12 \pm_{0.05}^{0.04}$. f does not depend much on the geometry, but rather on the column density (Matt 2002). The observed value would correspond to a column density of a few $\times 10^{23} \text{ cm}^{-2}$, for which values around 100 eV of the EW are expected (a value of about 20 eV is instead expected for $1.9 \times 10^{24} \text{ cm}^{-2}$). The observed EW is instead about 13 eV. It is then possible that the matter is very inhomogeneous, with a denser blob just on the line of sight (which is what the fit can measure) but an average optical depth an order of magnitude less, and a covering factor, taking into account the uncertainties on the power law index, of about 0.1–0.2. The lower (with respect to the line of sight) average column density, along with the relative small covering factor, would explain the failure of the Matt et al. (1999) model in fitting the data.

Because there is evidence that the absorbing material has a covering factor less than 1, part of the X-ray illuminated surface should be directly visible, producing a Compton reflection component (George & Fabian 1991; Matt, Perola & Piro 1991) as commonly observed in Compton-thick AGN (Matt et al. 2000 and references therein). As discussed above, the average column density is possibly as low as a few $\times 10^{23} \text{ cm}^{-2}$; however, below the iron line energy the reflection component for this column density is very similar to that for Compton-thick matter (Matt et al. 2003). This component could therefore account for the excess emission below 5 keV (see Fig. 2, where the whole 0.3–13 keV spectrum is shown, after being fitted with the baseline model), and down to about 2 keV (the further excess at lower energies should have a different origin). Fitting the 2–13 keV spectrum with the baseline model gives $\chi^2=104.9/68$ d.o.f., and a very flat ($\Gamma=0.6$) power law. The addition of a pure Compton reflection component (with the photon index linked to that of the absorbed power law, and fixed to 1.6) improves the fit significantly, giving $\chi^2=79.9/68$ d.o.f. The value of R , 0.003, implies that the visible part of the illuminated matter is very small (R is equal to 1 for 2π visible solid angle, i.e. a covering factor of 0.5). As the source lies on the Galactic plane, absorption from interstellar matter is likely to be

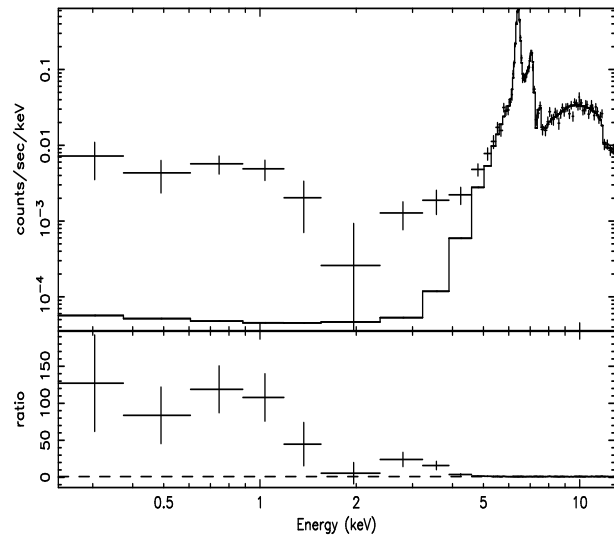


Figure 2. The overall 0.3–13 keV time integrated spectrum fitted with the baseline model.

significant. We then added an absorption component, but the fit does not significantly improve ($\chi^2=77.9/68$ d.o.f.). The best-fit face value for the column density of this further absorber is about $5 \times 10^{22} \text{ cm}^{-2}$, and $R=0.0045$. (If this is indeed the column density of the interstellar absorption, the emission below 2 keV is likely due to another, nearby confusing source.) The other parameters are similar to those listed in Table 1. The iron line EW with respect to the reflection component is very large, ~ 28 keV, implying that almost all of the line is related to the transmitted component. Of course, part of the excess emission may be due to photons scattered in transmission rather than reflection, i.e. escaping from the far side (with respect to the X-ray source) of the obscuring matter.

The small value of R may, at the first glance, appear rather surprising, given the value of the covering factor deduced from the iron line EW and the CS (about 0.1). It may be explained if, e.g., the absorber has a flat configuration (similar to the ‘torus’ envisaged in Unification Models for AGN), seen at high inclination.

3.3 Time resolved spectra

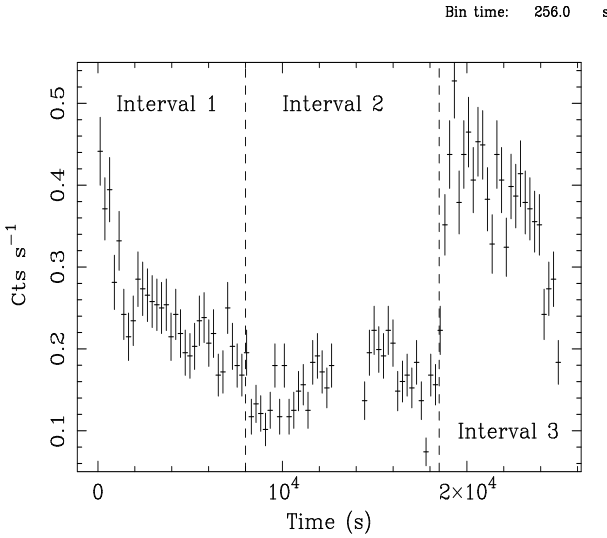
IGR J16318-4848 exhibits a complex variability pattern during the XMM-Newton observation (see Fig. 3). The pn flux varied by a factor of 2.5 during the first 8 ks, stabilized at a constant level of $\simeq 0.15 \text{ s}^{-1}$ (0.5–15 keV band) for the next 13 ks and then underwent a sudden burst, brightening by a factor $\simeq 3$ within $\simeq 500$ –1000 s. This behavior is associated with spectral variability. In Fig. 4 we show the count spectra extracted in the 3 consecutive different time intervals highlighted in Fig. 3: 0–8 ks, 8–18.5 ks, and 18.5–25 ks (elapsed time) after the observation start. The exposure times corresponding to the three spectra are 7.7, 7.3 and 5.1 ks, respectively.

To test whether the flux variations are due to a change in the column density of the absorber, or rather in the properties of the primary emission, we performed three different fits: with Γ and the normalization of the power law kept fixed to the time integrated best fit values (baseline model), and

Table 1. Best fit results for the baseline model. Equivalent widths are calculated against the unabsorbed continuum.

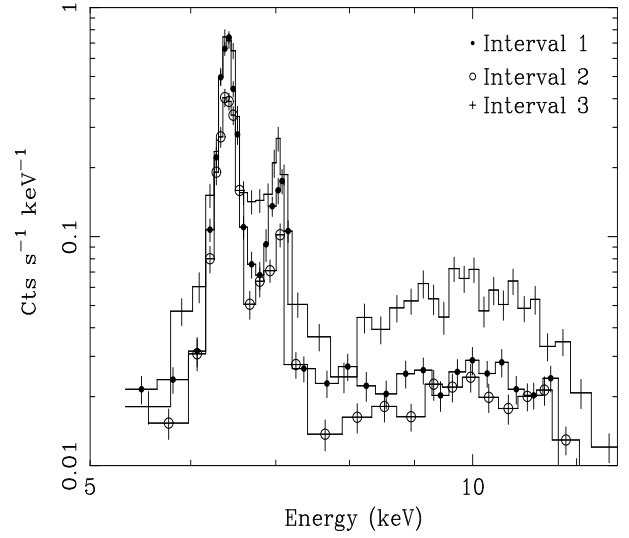
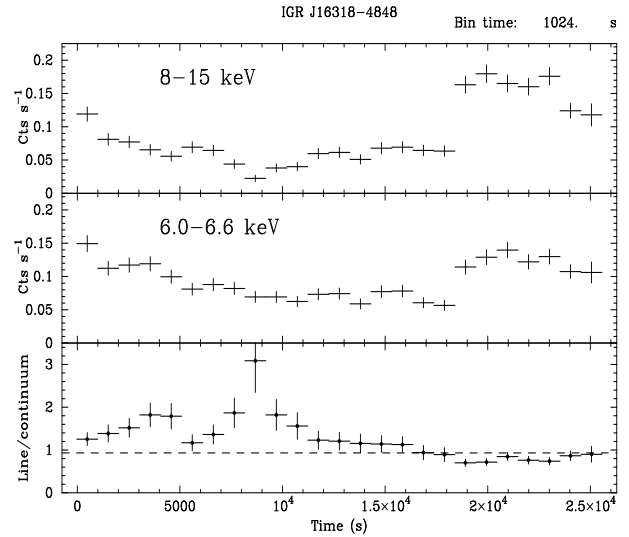
| | |
|--|---------------------------|
| Γ | $1.60^{+0.07}_{-0.11}$ |
| N_{H} (10^{24} cm $^{-2}$) | $1.91^{+0.03}_{-0.04}$ |
| A_{Fe}^a | $0.89^{+0.04}_{-0.03}$ |
| E (Fe K α) [keV] | $6.401^{+0.001}_{-0.001}$ |
| F (Fe K α) [10^{-5} ph cm $^{-2}$ s $^{-1}$] | $14.8^{+0.4}_{-0.6}$ |
| EW (Fe K α) [eV] | 13 |
| E (Fe K β) [keV] | $7.099^{+0.001}_{-0.006}$ |
| F (Fe K β) [10^{-5} ph cm $^{-2}$ s $^{-1}$] | $3.05^{+0.33}_{-0.38}$ |
| EW (FeK β) [eV] | 3 |
| E (Ni K α) [keV] | $7.45^{+0.05}_{-0.02}$ |
| F (Ni K α) [10^{-5} ph cm $^{-2}$ s $^{-1}$] | $0.85^{+0.19}_{-0.21}$ |
| EW (Ni K α) [eV] | 1 |
| F (Fe K α CS) [10^{-5} ph cm $^{-2}$ s $^{-1}$] | $1.88^{+0.59}_{-0.68}$ |

^a relative iron abundance in solar units (Anders & Grevesse 1989) by number.

**Figure 3.** pn light curve of the XMM-Newton observation of IGRJ 16318-4848 (single- and double-events; 0.5–15 keV energy band). The vertical lines indicate the time intervals, where time-resolved spectra discussed in Sect. 3.3 were extracted

N_{H} free to vary (model 1); with only Γ fixed and the normalization and N_{H} free (model 2); and with Γ and normalization free and N_{H} fixed (model 3). For the sake of simplicity, the fits have been performed in the 5–13 keV energy band. Hereinafter, all fits have been performed with the centroid energies of the emission lines (which do not exhibit significant evidence for variations among the time-resolved spectra) and the relative iron abundance kept fixed to the best fit values for the baseline model, as reported in Table 1. The resulting χ^2 are given in Table 2. While for the 2nd interval all models are acceptable, for the 1st and 3rd intervals model 1 is unacceptable, while model 2 and 3 are both acceptable. For model 2, the best fit values of N_{H} are (see also Table 3): $1.76^{+0.11}_{-0.10}$, $1.93^{+0.15}_{-0.12}$ and $2.06^{+0.09}_{-0.09}$. For model 3, the best fit values of Γ are: $1.85^{+0.20}_{-0.10}$, $1.55^{+0.19}$ and $1.30^{+0.18}$.

In Table 3 the best fit parameters for the absorbing col-

**Figure 4.** pn count spectra for the time-resolved intervals shown in Fig. 3**Figure 5.** The light curves in the 8–15 keV (upper panel) and 6.0–6.6 keV (middle panel) energy ranges. In the latter band, the contribution from the iron K α line is dominant. In the lower panel, the ratio of the two light curves is shown.

umn density and the 8–15 keV and line fluxes (obtained with model 2; the results on the line fluxes are similar if model 3 is adopted) are summarized. It is interesting to note that the fluxes of the lines are correlated with the flux of the continuum; the only exception is the Compton shoulder, but the errors are pretty large. This applies in particular for the spectra corresponding to Interval 2 (pre-burst) and 3 (post-burst). The ratios of the iron line fluxes between the post- and pre-burst phases (1.8 ± 0.2 and $2.4^{+0.8}_{-1.3}$ for K α and K β , respectively) are comparable with the average 8–15 keV continuum flux ratio between the same intervals (2.41 ± 0.04). To further explore the relation between the emission line and the continuum fluxes, in Fig. 5 the light curves for the 8–15 keV (which is dominated by the continuum) and the 6–6.6 keV (dominated by the iron K α line) are shown. The line varies on time scales as short as 1000 s, implying that the size

Table 2. $\chi^2/d.o.f.$ for the three time intervals for different models.

| | 1st int. | 2nd int. | 3rd int. |
|-----------------------|----------|----------|----------|
| Count rate (5-13 keV) | 0.36 | 0.27 | 0.54 |
| Γ , Norm fixed | 56.2/35 | 24.4/21 | 88.8/34 |
| Γ fixed | 41.9/34 | 21.8/20 | 37.3/33 |
| N_{H} fixed | 43.3/34 | 21.4/20 | 39.7/33 |

Table 3. Best fit results for the three time intervals, using model 2 (see text for details).

| | 1st int. | 2nd int. | 3rd int. |
|--------------------------------------|------------------------|------------------------|------------------------|
| N_{H}^a | $1.76^{+0.11}_{-0.10}$ | $1.93^{+0.15}_{-0.12}$ | $2.06^{+0.09}_{-0.09}$ |
| $F(8-15 \text{ keV})^b$ | 2.38 ± 0.04 | 2.23 ± 0.04 | 5.38 ± 0.03 |
| $F(\text{Fe } K\alpha)^c$ | $17.1^{+1.2}_{-0.9}$ | $10.1^{+0.8}_{-1.0}$ | $18.4^{+1.1}_{-1.7}$ |
| $F(\text{Fe } K\beta)^c$ | $3.9^{+0.6}_{-0.7}$ | $1.6^{+0.7}_{-0.4}$ | $3.8^{+0.8}_{-1.0}$ |
| $F(\text{Ni } K\alpha)^c$ | $0.8^{+0.5}_{-0.3}$ | $0.3^{+0.7}_{-0.3}$ | $1.5^{+0.7}_{-0.6}$ |
| $F(\text{Fe } K\alpha \text{ CS})^c$ | $2.1^{+0.8}_{-0.5}$ | $2.1^{+0.6}_{-0.8}$ | 2.0 ± 1.1 |

^a in units of 10^{24} cm^{-2}

^b in units of $10^{-11} \text{ erg cm}^{-2} \text{ s}^{-1}$

^c in units of $10^{-5} \text{ ph cm}^{-2} \text{ s}^{-1}$

of the emitting region cannot be larger than about 3×10^{13} cm, consistent with a scenario in which the absorbing matter is e.g. due to the stream of material flowing through the Lagrangian point in a Roche Lobe overflow, to eventually form an accretion disc.

The line flux follows the variations of the continuum, but not precisely, as it is clear from the line-to-continuum flux ratio (lower panel of Fig. 5), suggesting that on these time scales also the properties of the cold matter, i.e. the covering factor and/or the average column density, change.

4 SUMMARY

We have performed a detailed analysis of the XMM-Newton observation of IGR J16318-4848, in order to characterize the properties of the matter responsible for the obscuration along the line-of-sight and for the emission of Fe and Ni lines. Our results can be summarized as follows:

a) the line of sight material has a column density of about $2 \times 10^{24} \text{ cm}^{-2}$;

b) from the value of the Fe $K\alpha$ line EW and Compton Shoulder, an average column density of a few $\times 10^{23} \text{ cm}^{-2}$ (indicating dishomogeneous or blobby material) and a covering factor of about 0.1–0.2 are estimated;

c) the small value of the Compton reflection component suggests a flat configuration of the matter, with a large inclination angle;

d) the iron $K\alpha$ line varies on time scales as short as

1000 s, implying a size of the emitting region not exceeding $\sim 3 \times 10^{13}$ cm. The flux of the line roughly follows the variations of the continuum, but not exactly, suggesting a variation of the geometrical properties of the emitting region on similar time scales.

Finally, a few words on the putative “transient” nature of this source. A reanalysis of an archival 1994 ASCA observation (Murakami et al. 2003) points to a flux variation of a factor of just a few in about 8.5 years. The comparison between the flux measured by INTEGRAL in the 15–40 keV and by XMM-Newton in the 5–15 keV is not conclusive, given the large uncertainties associated with the determination of the intrinsic flux in such an absorbed source. Therefore, it cannot be ruled out that the XMM-Newton (and ASCA) observations represent already its normal flux level.

ACKNOWLEDGMENTS

This work is based on observations obtained with XMM-Newton, an ESA science mission with instruments and contributions directly funded by ESA Member States and the USA (NASA). The XMM-Newton Science Operation Center is gratefully acknowledged for having produced with unprecedented speed, and made publicly available ODF for the observation described in this paper.

REFERENCES

- Anders E., Grevesse N., 1989, *Geo. Cosm. Acta* 53, 197
 Anders E., Ebihara M., 1982, *Geo. Cosm. Acta* 46, 2363
 Balucinska-Church M., McCammon D., 1992, *ApJ*, 400, 699
 Bianchi S., et al., 2002, *A&A*, 396, 793
 Corvoisier T.-J., Walter R., Rodriguez J., Bouchet L., Loutouvinon A.A., *IAUC* 8063
 de Plaa J., den Hartog P.R., Kaastra J.S., in ‘t Zand J.J.M., Mendez M., Hermsen W., *ATEL* #119
 George I.M., Fabian A.C., 1991, *MNRAS*, 249, 352
 House L.L., 1969, *ApJS*, 18, 21
 Jansen F., et al., *A&A*, 361, L1
 Kaastra J.S., Mewe R., 1993, *A&AS*, 97, 443
 Matt G., Perola G. C., Piro L., 1991, *A&A*, 247, 25
 Matt G., et al., 2000, *MNRAS*, 318, 173
 Matt G., 2002, *MNRAS*, 337, 147
 Matt G., Guainazzi M., Maiolino R., 2003, *MNRAS*, in press (astro-ph/0302328)
 Molendi S., Bianchi S., Matt G., 2003, *MNRAS*, submitted
 Morrison R., McCammon D., 1983, *ApJ*, 270, 119
 Murakami H., Dotani T., Wijnands R., *IAUC* 8070
 Palmeri P., Mendoza C., Kallman T.R., Bautista M.A., 2002, *ApJ*, 577, L119
 Revnivtsev M., Sazonov S., Gilfanov M., Sunyaev R., 2003, *Ast. Letters*, in press (astro-ph/0303274)
 Schartel N., et al., *IAUC* 8072
 Stüder L., et al., *A&A*, 365, L18